Computing the Traversability of the Environment by Means of Sparse Convolutional 3D Neural Networks

Antonio Santo[1,2][a], Arturo Gil[1][b], David Valiente[1][c], Mónica Ballesta[1][d] and Adrián Peidró[1][e]
[1]*University Institute for Engineering Research, Miguel Hernández University, Avda. de la Universidad s/n, 03202 Elche (Alicante), Spain*
[2]*Valencian Graduate School and Research Network of Artificial Intelligence (valgrAI), Camí de Vera S/N, Edificio 3Q, 46022 Valencia, Spain*

Keywords: Autonomous Mobile Robots, Artificial Intelligence, Neural Networks, Point Clouds, Sparse Convolution.

Abstract: The correct assessment of the environment in terms of traversability is strictly necessary during the navigation task in autonomous mobile robots. In particular, navigating along unknown, natural and unstructured environments requires techniques to select which areas can be traversed by the robot. In order to increase the autonomy of the system's decisions, this paper proposes a method for the evaluation of 3D point clouds obtained by a LiDAR sensor in order to obtain the transitable areas, both in road and natural environments. Specifically, a trained sparse encoder-decoder configuration with rotation invariant features is proposed to replicate the input data by associating to each point the learned traversability features. Experimental results show the robustness and effectiveness of the proposed method in outdoor environments, improving the results of other approaches.

1 INTRODUCTION

The answer to the question "Where should I walk?", formulated in (Wellhausen et al., 2019) implicitly contains the understanding of everything that surrounds the robot in order to be able to navigate along the environment. This concept, which is assumed to be innate to humans, should be extrapolated to autonomous mobile robots, as it enables safe planning and navigation in various applications such as exploration of unknown environments, autonomous driving, search and rescue applications.

To date, path planning algorithms have been classified according to two fundamental concepts: a) the manner in which the space is defined and represented; b) the form in which the transitable zones are represented on the map. Thus, according to the first concept, different representations of the space can be found, such as: 2D occupancy maps (Moravec and Elfes, 1985), 3D voxel-based occupancy maps (Hornung et al., 2013; Oleynikova et al., 2017; Han et al., 2019) or elevation maps (DEM) (Langer et al., 1994), in which a probability value defines that a certain space is free or occupied, and may be traversed by the robot considering the physical parameters of the robot.

However, the classical approaches mentioned above are not sufficiently robust when applied to all types of environments (Xiao et al., 2022), since autonomous driving can be understood differently depending on the environment in which it is intended to navigate. Mainly in structured environments, the free space refers to regular roads, whereas for natural environments the concept is a bit abstract. The latter are environments complex and diverse and can hide invisible obstacles for the robots sensors.

This fact, together with a more sophisticated sensorization of the equipment (considering characteristics such as cost, resolution and lightness), justifies an approaching to compute traversability under a new paradigm: supervised machine learning, based on neural networks. Specifically, in recent years the use of LiDAR sensors in combination with Neural Networks has become popular. In particular, LiDAR sensors are immutable to different lighting conditions compared to other optical sensors such as cameras.

This paper proposes a contribution to the estima-

[a] https://orcid.org/0009-0006-0085-6273
[b] https://orcid.org/0000-0001-7811-8955
[c] https://orcid.org/0000-0002-2245-0542
[d] https://orcid.org/0000-0002-8029-5085
[e] https://orcid.org/0000-0002-4565-496X

Santo, A., Gil, A., Valiente, D., Ballesta, M. and Peidró, A.
Computing the Traversability of the Environment by Means of Sparse Convolutional 3D Neural Networks.
DOI: 10.5220/0012160300003543
In *Proceedings of the 20th International Conference on Informatics in Control, Automation and Robotics (ICINCO 2023) - Volume 1*, pages 383-393
ISBN: 978-989-758-670-5; ISSN: 2184-2809

tion of traversability in complex terrains using deep learning techniques, in particular segmentation methods of a scene described by means of 3D point clouds. The rest of the paper is organized as follows: Section 2 presents a summary of the most significant approaches in the field of Deep Learning for the calculation of traversability. Then, the concepts on which our method is based will be discussed and explained in Section 3. Finally, a set of experimental results is presented, that considers different types of environments that have been used in the training process. Finally, Section 5 presents the main conclusions that can be drawn from this approach.

2 RELATED WORK

This section describes some proposals in the field of traversability calculation using neural networks and machine learning. The contributions have been divided into two main blocks: conventional machine learning methods and methods based on the use of neural networks.

2.1 Conventional ML Methods

These group comprises algorithms that generally start from alternative representations of the input data, i.e., act on features extracted from the data which are considered to be discriminating for the problem to be solved. This strategy is employed in (Bellone et al., 2017), where stereo image pairs are used as input data. In (Vapnik, 1999), a study of the most discriminating geometric and appearance features for the traversability problem in urban environments is performed based on the training of an SVM classifier, concluding that features that include normal vectors are the most suitable for this task. In (Kragh et al., 2015), the calculation of features based on a local neighborhood for each point (obtained using a 3D LiDAR sensor) is proposed, in order to classify them into: soil, vegetation or object. In this proposal, an adaptive neighborhood radius is proposed to alleviate the loss of point density as a function of the distance to the sensor, which is inherent to LiDAR sensors. In this way, high resolutions are guaranteed at short distances, whereas noisy features at long distances are diminished.

One of the biggest problems with previous methods is the need for an expert to generate labels of the class to which each point belongs. Therefore, there are methods that automate this process by training the classifiers with simulated data such as (Martinez et al., 2020) which tries to describe point clouds extracted from the GAZEBO simulator from the analysis of the principal directions (PCA) in a given neighborhood environment.

2.2 Neural Networks

LiDAR sensors generate, at their output, the position of a set of 3D points. These 3D points correspond to the first reflection produced by an object when it is illuminated by a collimated laser beam. In relation to this fact, alternatives have been developed to efficiently work with three-dimensional data. For example, in (Velas et al., 2018), point clouds are transformed into multichannel images that store the depth, height and reflectivity of each point. These images are processed through dense convolutional layers to learn which areas are traversable. Another solution is presented in (Razani et al., 2021) where spherical projections of the point clouds are carried out. Next 2D convolutional layers are applied to solve a semantic segmentation problem. A different solution is presented in (Wang et al., 2017), where octal trees or *octrees* are used to reduce the complexity of the space described by the point clouds. In this manner, dense convolution operations are restricted to those octrees that are occupied. The same idea is extended in (Frey et al., 2022), where the traversability of the space is computed by means of a generalization of the convolution operation to *n*-dimensions and employing a sparse encoder-decoder setup (Choy et al., 2019).

On the other hand there are methods that combine the information provided by LiDAR with image information. (Gu et al., 2019) propose a road detection method by merging the color information provided by the camera and the range information obtained with the LiDAR. The point clouds are projected to their corresponding images and feed a 2D convolutional neural network. (Fan et al., 2020), fuses the features of both types of data once they have been extracted by different architectures of neural networks. (Chen et al., 2019) proposes a progressive adaptation of the LiDAR representation to make it more compatible with the visual information from the camera. To do so, the point cloud is transformed into an alternative representation where roads are more distinguishable.

3 PROPOSED APPROACH

This section defines the traversability problem. Next, a detailed description of the approach is presented.

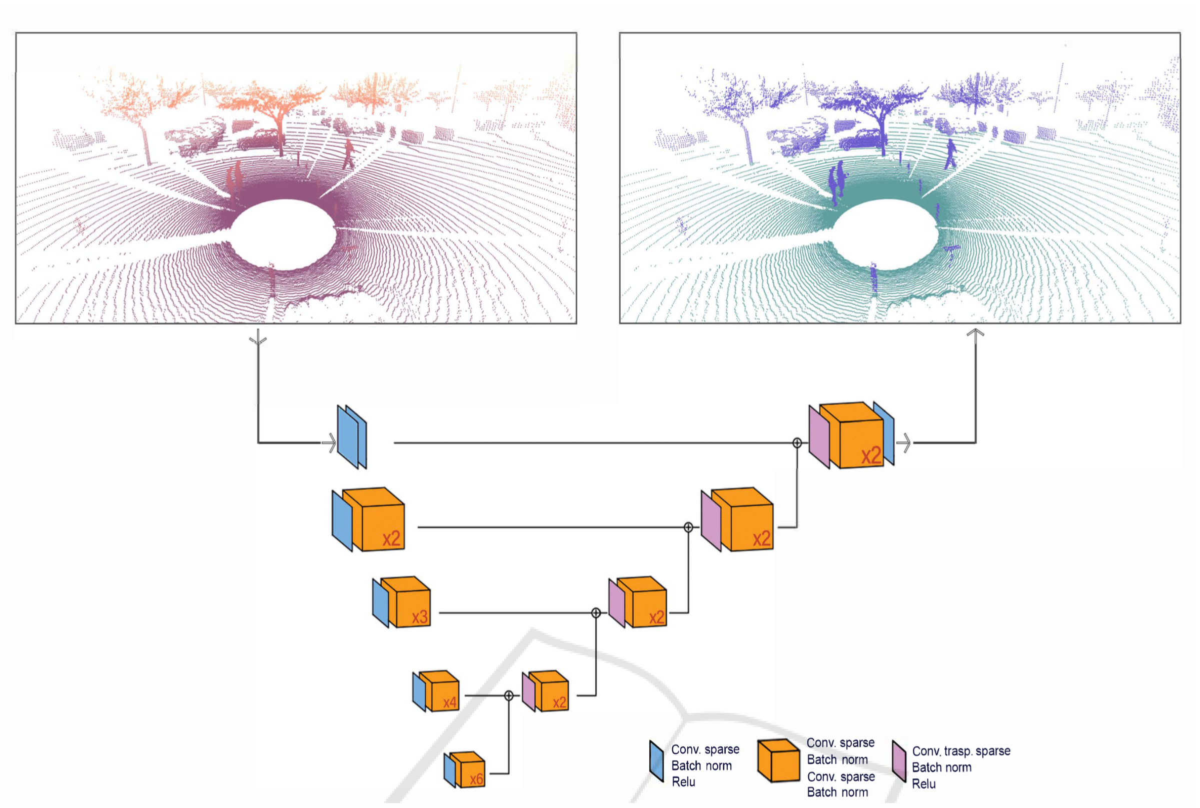

Figure 1: Encoder-decoder configuration employed, MinkUnet34 (Choy et al., 2019).

3.1 Problem Statement

The problem of traversability evaluation is considered as a semantic segmentation task. A point cloud B is defined as a set $B = \{(\vec{p}_i, \vec{f}_i, l_i),\ i = 1, \ldots, N\}$, where N is the total number of points in the cloud, each point with coordinates $\vec{p}_i \in \mathbb{R}^3$ expressed in the LiDAR reference frame. The traversability condition of each point is denoted as l_i. We consider that each point is associated to a feature vector $\vec{f}_i \in \mathbb{R}^{d_{\text{in}}}$, being d_{in} the dimensionality of the input features associated with each point in the cloud. Each point originated by the LiDAR sensor is considered to have coordinates $\vec{p}_i = (x_i, y_i, x_i)$, according to the coordinate system of the LiDAR sensor itself. The aim is to infer a classification $l_{\text{i}} \in [0, 1]$ that represents the traversavility condition of the LiDAR point, that is: traversable (1) or not traversable (0). Thus, the problem can be defined as a point-wise binary classification problem.

3.2 Sparse Convolution

The discrete convolution operation was originally born in the field of signal processing. However, it is profusely used in image processing and in convolutional Neural Networks.

This type of neural networks, despite being computationally expensive, show great results in problems such as image classification and segmentation. However, their possible application to sparse data, such as point clouds, understanding sparsity as the distancing of the set of values that constitute the data, would be computationally inefficient due to their sequential and iterative nature. The operations to be performed would increase by a cubic factor. As a result, the generalization of the 2D convolution in images gives rise to the sparse convolution operation.

This type of discrete convolution allows to focus the convolution kernel on those discretized spaces where a non-zero value exists, thus departing from the classical constant displacement of a 2D mask when the convolution operation is applied on images. This idea is particularly efficient in point clouds since there are many void zones in the cloud and, therefore, the convolution operation on those areas would only result in unnecessary time and resource consumption.

Therefore, given any point cloud B, a sparse tensor $\mathbf{S}$ is defined, in turn, formed by two tensors $\mathbf{S}(\mathbf{T}_{\text{C}}, \mathbf{T}_{\text{F}})$:

- $\mathbf{T}_{\text{C}}$ is defined as a function of the coordinates of the points that constitute the original cloud $B = \{(\vec{p}_i, \vec{f}_i, l_i),\ i = 1, \ldots, N\}$. An integer part function is applied to discretize the space. The points are modified according to a scaling factor, v, that determines the discretization of the space. In addition, the batch b_i to which each point cloud belongs is added to facilitate the training of the network. Thus, the tensor $\mathbf{T}_\mathrm{C}$ is defined as:

$$\mathbf{T}_\mathrm{C} = \begin{bmatrix} b_1 & \bar{p}_1 \\ \vdots & \vdots \\ b_N & \bar{p}_M \end{bmatrix} \tag{1}$$

$$\text{with } \bar{p}_j = floor(\vec{p}_i) = floor\left(\frac{x_i}{v}, \frac{y_i}{v}, \frac{z_i}{v}\right)$$

As a result, m points belonging to the point cloud could be discretized in the same voxel $\bar{p}_j$. Each of the m points having a different feature vector $\vec{f}_i$.

- $\mathbf{T}_\mathrm{F}$ stores and averages the features $\vec{f}_i$ associated with the m points, that share the same space, i.e. belong to the same voxel, $\bar{p}_j$, after applying the scale factor v and the integer part function.

$$\mathbf{T}_\mathrm{F} = \begin{bmatrix} \bar{f}_1 \\ \vdots \\ \bar{f}_M \end{bmatrix} \tag{2}$$

$$\begin{aligned} \text{where } \bar{f}_j &= \frac{1}{m}\sum_{i=1}^{m} \vec{f}_i \\ \forall & \quad \vec{f}_i \in \bar{p}_j \end{aligned}$$

The processing of the input data is carried out using the Minkowski Engine library[1] (Choy et al., 2019).

3.3 Sparse 3D Neural Networks

The method presented in this document uses a neural network with an encoder-decoder configuration, whose implementation is a sparse variety of the convolutional neural network Resnet20 (He et al., 2016) and the U-net architecture (Ronneberger et al., 2015). Therefore, the network is mainly divided into two parts:

- **Encoder.** The encoding part of the network is in charge of generating point descriptors based on the 3D sparse convolution of the features belonging to each point. In this case, during this research, different combinations of input features were tested, such as: the coordinates of each point $\vec{p}_i = (x_i, y_i, z_i)$, the normal vectors of each point $\vec{N}_i = (n_x, n_y, n_z)_i$ and several combinations of these features. Finally, in this approach the feature vector is defined as: $\vec{f}_i = (n_z, Z)$ where n_z is the Z coordinate of the normal unit vector $\vec{N}_i$ and the normalized coordinate $Z \in [0,1]$. This feature vector includes a natural invariance to rotation to the point cloud along the vertical axis and, in the experiments carried out, allowed to obtain the best results.
- **Decoder.** The decoding part of the network tries to reconstruct and extrapolate the latent information generated by the encoder to the coordinates of the input point cloud. For this purpose, transposed convolution layers are used.

[1]https://github.com/NVIDIA/MinkowskiEngine

The network configuration is shown in Figure 1. The figure represents different levels of the neural network in a top-down way, by means of sparse convolutions and sparse residual blocks. In addition, once the encoder is finished, the scheme continues in an ascending way through the concatenation of the descriptors of different levels, indicated by the symbol $\oplus$, and transposed convolutions to recover the original shape of the input point cloud.

4 EXPERIMENTAL RESULTS

This section presents the experimental results obtained by the proposed method under different training configurations.

4.1 Datasets

A set of freely available databases have been used for training, validation and testing of the neural network, in particular:

1) SemanticKITTI: This is a dataset based on the KITTI Vision Benchmark (Geiger et al., 2012). It combines odometry positions and point clouds from different paths through the city of Karlsruhe, Germany, collected by the Velodyne HDL-64E sensor model. It includes, in total, 22 urban sequences, describing highly structured environments. Ten of these sequences contain labels for each point, oriented to semantic segmentation problems.

2) Rellis-3D (Jiang et al., 2021): It consists of a dataset of 13,556 point clouds divided into 4 distinct sequences captured by means of an OS1-64 LiDAR. There are labels for each point, and unlike the SemanticKITTI it describes highly unstructured environments and rural roads.

3) SemanticUSL (Jiang and Saripalli, 2021): This dataset, employed a Clearpath Warthog equipped with an OS1-64 LiDAR. It includes footage of the campus and research facilities of the University of Texas. It contains 1200 point clouds labeled under the same

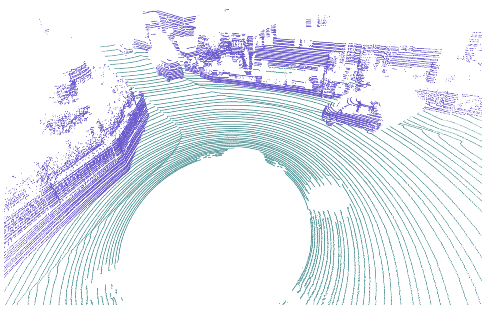
(a) KITTI translated.

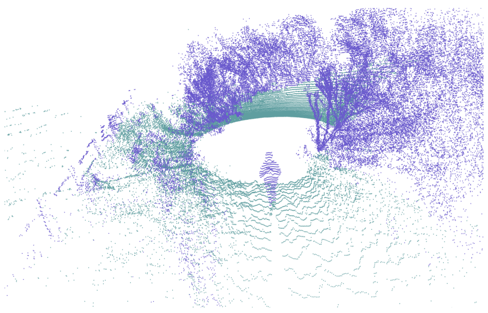
(b) Rellis-3D translated.

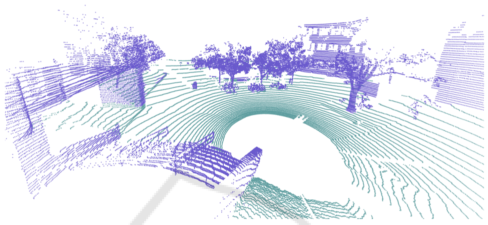
(c) SemanticUSL translated.

Figure 2: Translation of the original labels to two traversability labels.

format as the SemanticKITTI including road scenes, pedestrian streets and natural environments.

All the mentioned databases contain, approximately, 25 different labels to which a point can belong. These labels include semantic concepts such as: bush, mud, asphalt, sidewalk... etc. The datasets were relabeled, attending to the traversability condition, giving, as a result, only two classes ("traversable" and "non-traversable"). Figure 2 shows the modifications made to the data to fit a binary segmentation problem. The original classes that have been converted to the "traversable" class are: sidewalk, asphalt, low vegetation or grass, dirt, cement and mud. The classes that have been converted to the class "non-traversable" are: tree, person, car, truck, building, among others.

4.2 Implementation Details

The neural network model is implemented using the Minkowski Engine (Choy et al., 2019) and Pytorch. The network training has been performed using two NVIDIA 3090 TURBO graphics cards and a termination criterion that optimizes the F1 metric on a given balanced validation set. All the code, including a guide to the changes made to the original datasets mentioned in section 4.1, has been developed in Python and is available at `https://github.com/ARVCUMH/transitability_minkowski.git`

As for the training parameters we have employed a learning ratio of 0.01 and the stochastic gradient descent method (SGD) as the optimizer. In addition, given the binary nature of our approach we employed the binary cross-entropy loss function.

In order to reduce the feature processing time in a real application, the point clouds are voxelized at 3 centimeters. Thus the calculation of the normal vectors is supported by the search of the 6 nearest neighbors of each point by means of a KDtree algorithm implemented by open3D library (Zhou et al., 2018).

4.3 Training Network

The training stage of the aforementioned datasets has been carried out using only some SemanticKITTI sequences and all of the Rellis-3D sequences. The reason for this choice is to have a balanced number of training examples including, equally, urban, unstructured and natural environments. This prevents the network from specializing in a particular type of environment. The use of the SemanticUSL database is limited exclusively to test processes in order to demonstrate the generalization capabilities of the network in environments never seen during training.

In addition, during the experiments, the network has been trained using variations of the scaling parameter v to discretize the space, as it will be shown in the following sections.

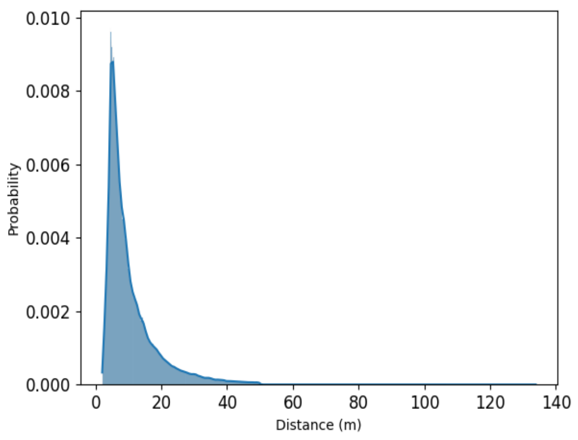

Figure 3: Probability density function according to the distance of each point to the sensor.

4.4 Distance Effect

By studying how LiDAR planes interact with the surrounding environment, it is clear that the distance, d, between consecutive LiDAR planes and the ground plane depends on the angle formed by the intersection of the two planes mentioned above, α, and the height, h, at which the LiDAR is located. This relationship is governed by:

$$d = \frac{h}{\tan \alpha} \tag{3}$$

Thus, at very far distances, the different laser planes are far apart. This effect is easy to appreciate in Figure 2. Consequently, the description of some regions in the robot environment is very inaccurate, since the LiDAR point density is very low. This concept is represented in Figure 3, which shows the probability of the existence of points based on the distance to the sensor. The probability density function is computed based on the observations of 100 point clouds. It can be seen how, above 45 meters, the probability of finding points is almost zero. Therefore, as a solution, it was proposed to consider only the points that are within a radius of 45 meters from the sensor and, all the evaluations have been performed under this condition.

4.5 Quantitative Evaluation

Figure 4 presents the results in terms of precision and recall. For this purpose, inferences have been made on all the point clouds that make up the test dataset. The classification of each point inferred by the network is compared with its ground truth, giving rise to true positives, true negatives, false positives and false negatives. Figures 4(a) and 4(c), present the results in urban and structured environments corresponding to SemanticKITTI and USL datasets. In both figures, the precision-recall curve is very close to the maximum (upper right corner). Therefore we can assume that the trained models learn the traversable and non-traversable zones very consistently, achieving accuracy and recall values higher than 95% for certain working points. Moreover, these curves show that the performance of the network does not depend on the discretization parameter v (size of voxel, or scale parameter), since very similar values are achieved.

On the other hand, Figure 4(b) presents the results when the method is applied to an unstructured environment. As expected, the results suggest that it is more difficult to correctly infer which areas are traversable. Likewise, in this case, the discretization of the point cloud space is a determining factor, since differences in performance are observed depending on this factor. The improvement of some voxels with respect to others does not seem to follow a logical order for these specific environments.

Table 1 shows in detail the performance metrics obtained according to the scale factor mentioned above. It can be observed in a more analytical way how the datasets describing urban environments lead to very similar results (SemanticKITTI, SemanticUSL). However, in highly unstructured datasets the performance of the neural network is lower and more dependent on the discretization of the point cloud.

Table 1: Results with different discretizations of the space on the described databases.

Dataset	Voxel	F1	Acc.	MIOU
Rellis3D		0.72	0.82	0.58
Kitti	0.05	0.97	0.97	0.94
USL		0.91	0.90	0.83
Rellis3D		0.72	0.83	0.57
Kitti	0.1	0.97	0.97	0.95
USL		0.93	0.93	0.87
Rellis3D		0.79	0.85	0.66
Kitti	0.2	0.97	0.97	0.94
USL		0.93	0.93	0.87
Rellis3D		0.79	0.86	0.66
Kitti	0.35	0.97	0.97	0.94
USL		0.95	0.95	0.91
Rellis3D		0.78	0.84	0.65
Kitti	0.5	0.97	0.97	0.93
USL		0.94	0.94	0.89

In addition, a comparison has been made with other results found in the literature (Table 2). The comparison presented in Table 2 includes different methods focused on semantic segmentation. According to (Fusaro et al., 2023), the datasets were adapted to a binary problem as we do in section 4.1.

Finally, an experiment was carried out with the aim of demonstrating the invariance of the obtained features. Figure 5 shows the variation of the precision

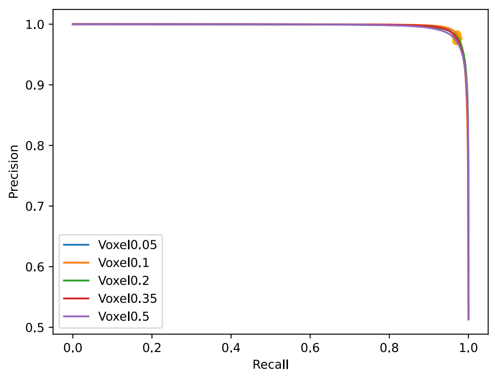

(a) P-R curve on the SemanticKITTI dataset.

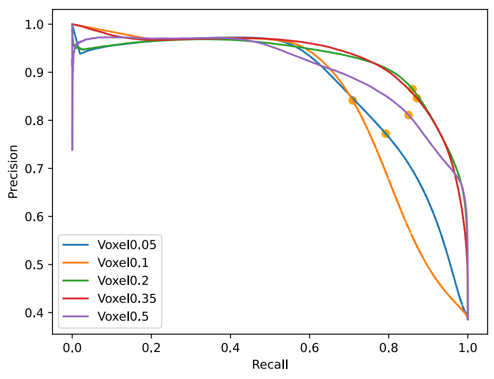

(b) P-R curve on the Rellis-3D dataset.

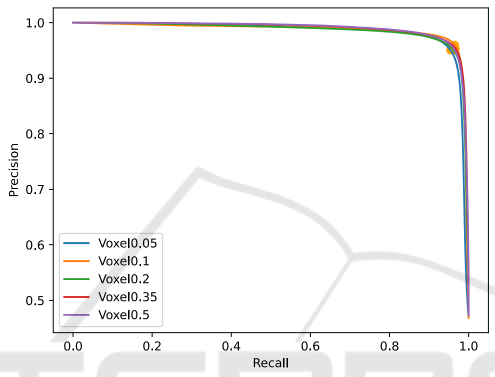

(c) P-R curve on the USLSemantic dataset.

Figure 4: Precision-Recall curves of network inference on test data.

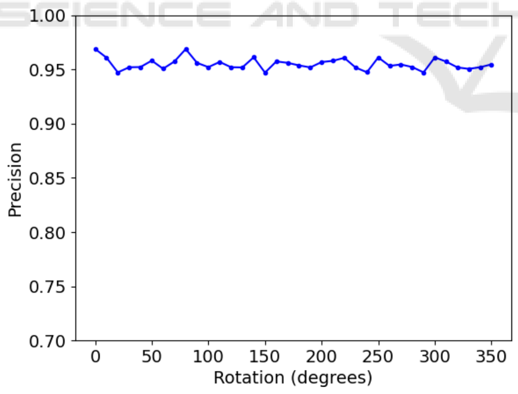

(a) Precision metric in relation to rotation.

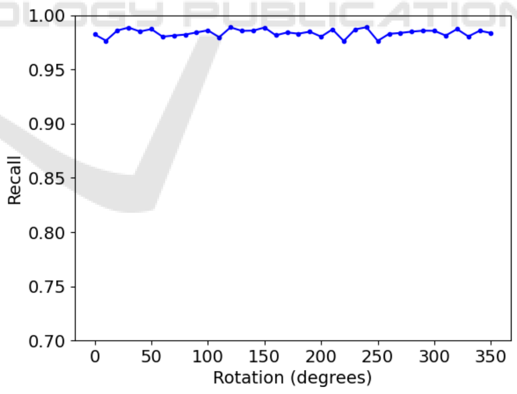

(b) Recall metric in relation to rotation.

Figure 5: Rotationally invariant results.

and recall metrics of a point cloud rotated between 0 and 360 degrees. Ideally the graph should present a completely horizontal line, however, due to the different discretization of the space when rotating, the results vary very slightly, and it can be considered to be invariant to rotation.

4.6 Qualitative Evaluation

In Figure 6, the results are presented in a visual form, in which the parameters that compose the confusion matrix are shown in different colors: true positives (green), true negatives (purple), false positives (red) and false negatives (orange). Figures 6(a), 6(c) and 6(e) represent a perfectly labeled point clouds of the

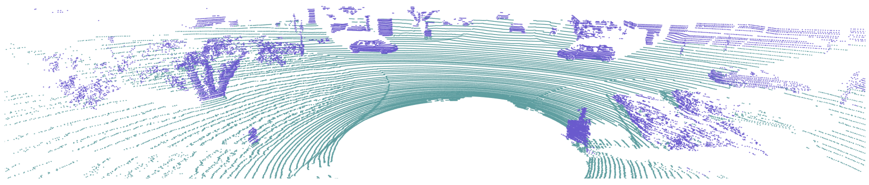
(a) Labeled point cloud from SemanticKITTI dataset.

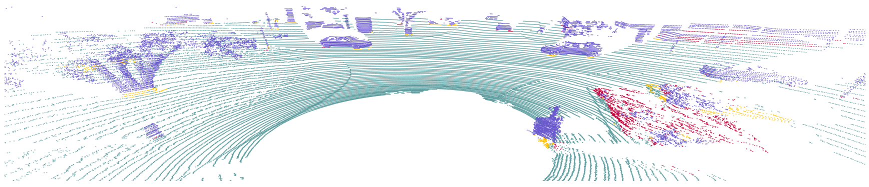
(b) Network inference from SemanticKITTI dataset.

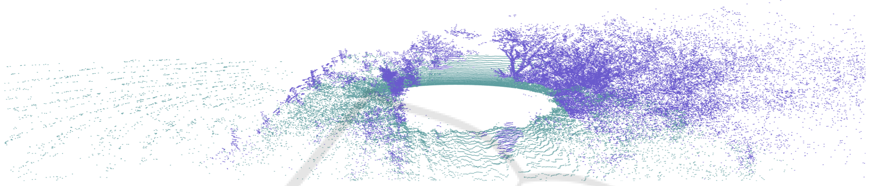
(c) Labeled point cloud Rellis-3D dataset.

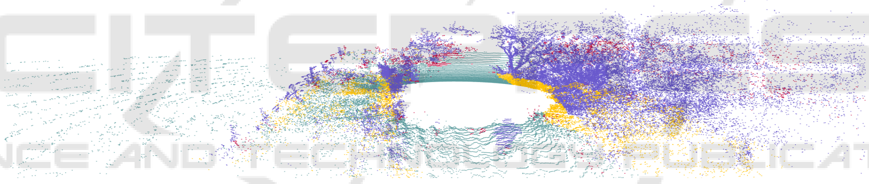
(d) Network inference from Rellis-3D dataset.

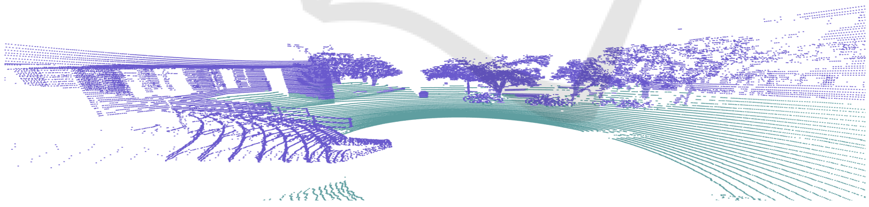
(e) Labeled point cloud from USL dataset.

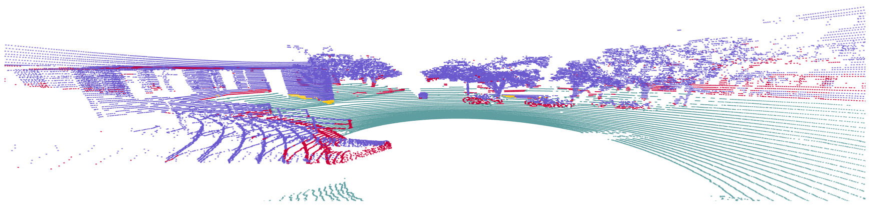
(f) Network inference from USL dataset.

Figure 6: Visual representation of the inference results of the network. Green: true positives (TP). Purple: true negatives (TN). Red: false positives (FP). Orange: false negatives (FN).

different datasets with which the method has been evaluated. On the other hand, Figure 6(b), 6(d) and 6(f) represent the neural network inferences with the errors in orange and red and the hits in green and pur-

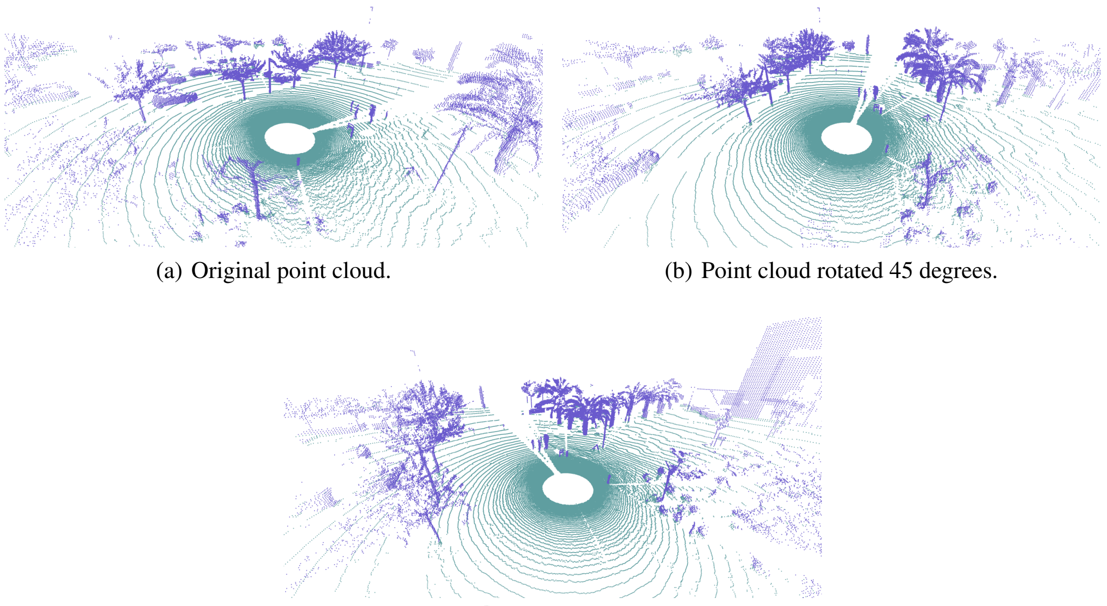
(a) Original point cloud. (b) Point cloud rotated 45 degrees.

(c) Point cloud rotated 90 degrees.

Figure 7: Inference invariant to rotation.

Table 2: Results of different approaches on SemanticKITTI sequences 0-10. With [1]: (Redmon and Farhadi, 2018), [2]: (Wu et al., 2018), [3]: (Wu et al., 2019), [4]: (Qi et al., 2017), [5]: (Fusaro et al., 2023).

Method	Accuracy	F1	mIoU
[1]	93.4	93.0	87.4
[2]	90.1	89.4	81.4
[3]	92.3	91.9	85.5
[4]	90.0	93.0	87.4
[5]	89.2	91.4	84.9
Ours	**96.6**	**95.9**	**92.3**

ple as described above. False positives tend to appear in highly unstructured areas. False negatives appear near the edges found between two adjacent geometries.

At this point, it is important to consider that false positives (classified by the network as traversable, but which are really not traversable) are really dangerous in a robot navigation task.

In the same way that before it has been shown that the method is invariant to rotation in a general way, we can directly observe this fact in Figure 7. This figure shows the inferences of the neural network for the same point cloud rotated 45 and 90 degrees in Figures 7(b) and Figure 7(c) respectively.

5 CONCLUSION

In this paper have been presented a method for traversability estimation in point clouds using a sparse neural network with an encoder-decoder configuration. An analysis in terms of voxel size has been performed on different datasets.

The results obtained demonstrate a high robustness of the solution both in highly structured and natural environments and improve the results of the approaches that are found in the literature. In particular, the study shows that the estimation of traversability performs very well in semi-structured environments (SemanticKITTI, SemanticUSL). It is a more complicated task in highly disordered natural environments (Rellis-3D). It has also been shown that the results are invariant to changes in rotation in the same environment, giving rise to small variations that do not generally affect the assessment of the traversability of the space.

As future work, we plan to merge the visual information with the LiDAR representation to make the method more consistent. In addition, we plan to test the neural network on different robots with different sensors. Finally, we plan to address the problem of space traversability under a continuous (non-binary) paradigm that depends in some way also on the physical characteristics of the robot and not only on the terrain.

ACKNOWLEDGEMENTS

This work has been funded by the ValgrAI Foundation, Valencian Graduate School and Research Network of Artificial Intelligence through a predoctoral grant. In addition, this publication is part of the project TED2021-130901B-I00, funded by MCIN/AEI/10.13039/501100011033 and by the European Union "NextGenerationE"/PRTR" and of the projects PROMETEO/2021/075, and GIGE/2021/150, funded by the Generalitat Valenciana.

REFERENCES

Bellone, M., Reina, G., Caltagirone, L., and Wahde, M. (2017). Learning traversability from point clouds in challenging scenarios. *IEEE Transactions on Intelligent Transportation Systems*, 19(1):296–305.

Chen, Z., Zhang, J., and Tao, D. (2019). Progressive lidar adaptation for road detection. *IEEE/CAA Journal of Automatica Sinica*, 6(3):693–702.

Choy, C., Gwak, J., and Savarese, S. (2019). 4D spatio-temporal convnets: Minkowski convolutional neural networks. In *Proceedings of the IEEE/CVF conference on computer vision and pattern recognition*, pages 3075–3084.

Fan, R., Wang, H., Cai, P., and Liu, M. (2020). Sne-roadseg: Incorporating surface normal information into semantic segmentation for accurate freespace detection. In *European Conference on Computer Vision*, pages 340–356. Springer.

Frey, J., Hoeller, D., Khattak, S., and Hutter, M. (2022). Locomotion policy guided traversability learning using volumetric representations of complex environments. In *2022 IEEE/RSJ Int. Conf. on Intelligent Robots and Systems (IROS)*, pages 5722–5729. IEEE.

Fusaro, D., Olivastri, E., Evangelista, D., Imperoli, M., Menegatti, E., and Pretto, A. (2023). Pushing the limits of learning-based traversability analysis for autonomous driving on cpu. In *Intelligent Autonomous Systems 17: Proceedings of the 17th Int. Conf. IAS-17*, pages 529–545. Springer.

Geiger, A., Lenz, P., and Urtasun, R. (2012). Are we ready for autonomous driving? the kitti vision benchmark suite. In *2012 IEEE conference on computer vision and pattern recognition*, pages 3354–3361. IEEE.

Gu, S., Zhang, Y., Tang, J., Yang, J., and Kong, H. (2019). Road detection through crf based lidar-camera fusion. In *2019 International Conference on Robotics and Automation (ICRA)*, pages 3832–3838. IEEE.

Han, L., Gao, F., Zhou, B., and Shen, S. (2019). Fiesta: Fast incremental euclidean distance fields for online motion planning of aerial robots. In *2019 IEEE/RSJ Int. Conf. on Intelligent Robots and Systems (IROS)*, pages 4423–4430. IEEE.

He, K., Zhang, X., Ren, S., and Sun, J. (2016). Deep residual learning for image recognition. In *Proceedings of the IEEE conference on computer vision and pattern recognition*, pages 770–778.

Hornung, A., Wurm, K. M., Bennewitz, M., Stachniss, C., and Burgard, W. (2013). Octomap: An efficient probabilistic 3D mapping framework based on octrees. *Autonomous robots*, 34:189–206.

Jiang, P., Osteen, P., Wigness, M., and Saripalli, S. (2021). Rellis-3D dataset: Data, benchmarks and analysis. In *2021 IEEE Int. Conf. on robotics and automation (ICRA)*, pages 1110–1116. IEEE.

Jiang, P. and Saripalli, S. (2021). Lidarnet: A boundary-aware domain adaptation model for point cloud semantic segmentation. In *2021 IEEE Int. Conf. on Robotics and Automation (ICRA)*, pages 2457–2464. IEEE.

Kragh, M., Jørgensen, R. N., and Pedersen, H. (2015). Object detection and terrain classification in agricultural fields using 3D lidar data. In *Computer Vision Systems: 10th Int. Conf., ICVS 2015, Copenhagen, Denmark, July 6-9, 2015, Proceedings*, pages 188–197. Springer.

Langer, D., Rosenblatt, J., and Hebert, M. (1994). A behavior-based system for off-road navigation. *IEEE Transactions on Robotics and Automation*, 10(6):776–783.

Martinez, J. L., Moran, M., Morales, J., Robles, A., and Sanchez, M. (2020). Supervised learning of natural-terrain traversability with synthetic 3D laser scans. *Applied Sciences*, 10(3):1140.

Moravec, H. and Elfes, A. (1985). High resolution maps from wide angle sonar. In *Proceedings. 1985 IEEE Int. Conf. on robotics and automation*, volume 2, pages 116–121. IEEE.

Oleynikova, H., Taylor, Z., Fehr, M., Siegwart, R., and Nieto, J. (2017). Voxblox: Incremental 3D euclidean signed distance fields for on-board mav planning. In *2017 IEEE/RSJ Int. Conf. on Intelligent Robots and Systems (IROS)*, pages 1366–1373. IEEE.

Qi, C. R., Su, H., Mo, K., and Guibas, L. J. (2017). Pointnet: Deep learning on point sets for 3D classification and segmentation. In *Proceedings of the IEEE conference on computer vision and pattern recognition*, pages 652–660.

Razani, R., Cheng, R., Taghavi, E., and Bingbing, L. (2021). Lite-hdseg: Lidar semantic segmentation using lite harmonic dense convolutions. In *2021 IEEE Int. Conf. on Robotics and Automation (ICRA)*, pages 9550–9556. IEEE.

Redmon, J. and Farhadi, A. (2018). Yolov3: An incremental improvement. *arXiv preprint arXiv:1804.02767*.

Ronneberger, O., Fischer, P., and Brox, T. (2015). U-net: Convolutional networks for biomedical image segmentation. In *Medical Image Computing and Computer-Assisted Intervention–MICCAI 2015: 18th Int. Conf., Munich, Germany, October 5-9, 2015, Proceedings, Part III 18*, pages 234–241. Springer.

Vapnik, V. (1999). *The nature of statistical learning theory*. Springer science & business media.

Velas, M., Spanel, M., Hradis, M., and Herout, A. (2018). CNN for very fast ground segmentation in velodyne lidar data. In *2018 IEEE Int. Conf. on Autonomous Robot Systems and Competitions (ICARSC)*, pages 97–103. IEEE.

Wang, P.-S., Liu, Y., Guo, Y.-X., Sun, C.-Y., and Tong, X. (2017). O-CNN: Octree-based convolutional neural networks for 3D shape analysis. *ACM Transactions On Graphics (TOG)*, 36(4):1–11.

Wellhausen, L., Dosovitskiy, A., Ranftl, R., Walas, K., Cadena, C., and Hutter, M. (2019). Where should i walk? predicting terrain properties from images via self-supervised learning. *IEEE Robotics and Automation Letters*, 4(2):1509–1516.

Wu, B., Wan, A., Yue, X., and Keutzer, K. (2018). Squeezeseg: Convolutional neural nets with recurrent crf for real-time road-object segmentation from 3D lidar point cloud. In *2018 IEEE Int. Conf. on robotics and automation (ICRA)*, pages 1887–1893. IEEE.

Wu, B., Zhou, X., Zhao, S., Yue, X., and Keutzer, K. (2019). Squeezesegv2: Improved model structure and unsupervised domain adaptation for road-object segmentation from a lidar point cloud. In *2019 Int. Conf. on Robotics and Automation (ICRA)*, pages 4376–4382. IEEE.

Xiao, X., Liu, B., Warnell, G., and Stone, P. (2022). Motion planning and control for mobile robot navigation using machine learning: a survey. *Autonomous Robots*, 46(5):569–597.

Zhou, Q.-Y., Park, J., and Koltun, V. (2018). Open3d: A modern library for 3d data processing. *arXiv preprint arXiv:1801.09847*.